Cover Page

Principal Investigator: Dr. David Ruzic
Postal Address: University of Illinois
216 Talbot Lab., 104 S. Wright St.
Urbana, IL 61801

Telephone: +1 (217) 333 0332
Email: druzic@illinois.edu

Funding Opportunity Announcement Number: DE-FOA-0000603
DOE/Office of Science Program Office: Office of Fusion Energy Science
DOE/Office of Science Program Office Technical Contact: Dr. Peter Pappano
DOE Award Number: DOE DE-SC0008587

Thermoelectric-Driven Liquid-Metal Plasma-Facing Structures (TELS) Final Report

David N. Ruzic

Center for Plasma Material Interactions, Department of Nuclear, Plasma and Radiological Engineering, University of Illinois, IL 61801 USA

1. Project Update
2. Task 1
    a. 1.3 Utilizing feedback from experiments and other flowing lithium work, create new TEMHD drive structures including systems with porous as opposed to open flow channels and systems suitable for NSTX upgrade, EAST and other interested fusion devices.
    b. 1.4 Test those structures eventually at higher magnetic fields (Task - 3) and under pulse plasma loads (Task - 2) as well as steady state heat fluxes.
    c. 1.6 Extend model to 3-D conjunction with work on others (eg. Neil Morley at UCLA)
    d. Additional progress on Task 1 Objectives
3. Task 2
    a. 2.4 Add diagnostics (TLP and OES) to combined device to look at vapor shielding and other effects of flowing lithium, and then other flowing metals under pulsed-plasma exposure.
4. Task 3
    a. 3.4 Compare flow behaviour to theory as a function of high magnetic field
5. Task 4
    a. 4.1 Measure seebeck coefficients of Sn and Sn-Li eutectics
    b. 4.2 Use and test Sn in the combined device
    c. 4.3 Use and measure the best Sn-Li mixture in the combined device.
6. No-cost extension period – 2015-2016 (Inputs from additional works)
7. Conclusion from the extended study
8. Further work.

1. Project Update

The Thermoelectric-Driven Liquid-Metal Plasma-Facing Structures (TELS) project was able to establish the experimental conditions necessary for flowing liquid metal surfaces in order to be utilized as surfaces facing fusion relevant energetic plasma flux. The work has also addressed additional developments along with progressing along the timeline detailed in the proposal. A no-cost extension was requested to conduct other relevant experiment- specifically regarding the

characterization droplet ejection during energetic plasma flux impact. A specially designed trench module, which could accommodate trenches with different aspect ratios was fabricated and installed in the TELS setup and plasma gun experiments were performed. Droplet ejection was characterized using high speed image acquisition and also surface mounted probes were used to characterize the plasma. The Gantt chart below had been provided with the original proposal, indicating the tasks to be performed in the third year of funding. These tasks are listed above in the progress report outline, and their progress status is detailed below.

Gantt Chart for all tasks during the three year project period

Task	Y1Q1	Q2	Q3	Q4	Y2Q1	Q2	Q3	Q4	Y3Q1	Q2	Q3	Q4
1.1												
1.2												
1.3												
1.4												
1.5												
1.6												
2.1												
2.2												
2.3												
2.4												
3.1												
3.2												
3.3												
3.4												
4.1												
4.2												
4.3												

2. Task 1

Modeling studies as well as the experimental trials have indicated that open trenches are ideal for utilizing the TEMHD effect to drive liquid lithium and hence the year 3 work was primarily focused on conducting trials using various open trench designs. The proposed design needed to be operated in tokamak relevant conditions, both in terms of handling highly energetic plasma fluxes as well as the geometrical orientation. Hence the test trials conducted to monitor the performance of the modules was broadly divided to two categories, in which the modules were operated in two different, but equally relevant conditions:

1. with flowing lithium in the DEVEX test stand, which was capable of generating ELM like energetic plasma fluxes.
2. operating at different orientations – by rotating the module with the flowing lithium to an arbitrary orientation (0 – 180 degrees).

Several iterations were made on the design for the trench filling mechanism. The current design is able to fill the trenches from the base, and can be manipulated over the top plane of the trenches, and thus can ensure proper filling. However, the design, being pressure driven, has the limitation that the entire pre-loaded volume is used up during the filling procedure, and thus cannot provide more lithium if necessary during the course of the experiment because the reservoir volume has to be matched with the trench volume in order to avoid over filling. To overcome this situation, an improved design with higher volume reservoir has been fabricated and is fully tested. In this design, the available volume of liquid lithium in the reservoir can be kept more than the total trench volume.

2.a, 2.b Task 1.4, 1.5 Progress

The open trench design was adapted and tested at various experimental conditions with suitable modifications relevant for each condition. Summary of the main versions of the TEMHD based flowing lithium systems (adaptations of the basic LiMIT design) is given below.

1. For HT-7 tokamak:

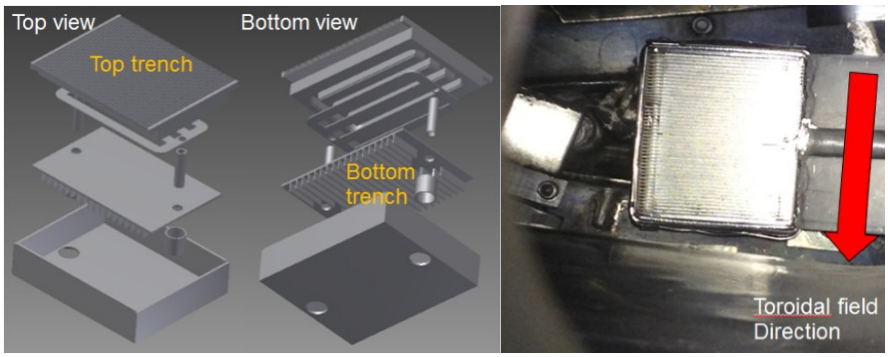

Fig. 1 The schematic of the trench assembly along with the lithium tray that has been installed and tested at the HT-7 tokamak in China (left). The top view of the installed lithium tray (right).

2. For Magnum-PSI

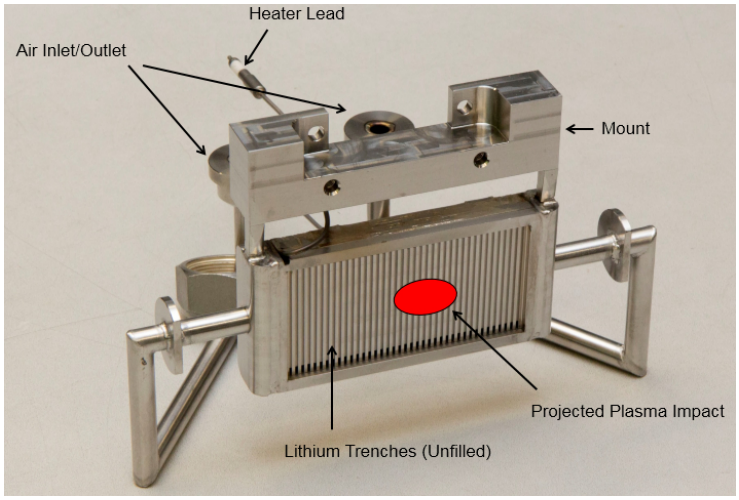

Fig. 2 The trench design for the module used for testing in the Magnum-PSI facility.

The Magnum-PSI facility is a linear plasma device capable of generating a parallel beam of ~ 25 MW/m^2 energy, which is comparable to the fusion relevant heat flux in tokamaks. The tests showed that the circulating liquid lithium was capable of safely handling "steady –state" long duration heat loads (5 s) by properly dissipating the incident heat energy.

3. The TELS assembly

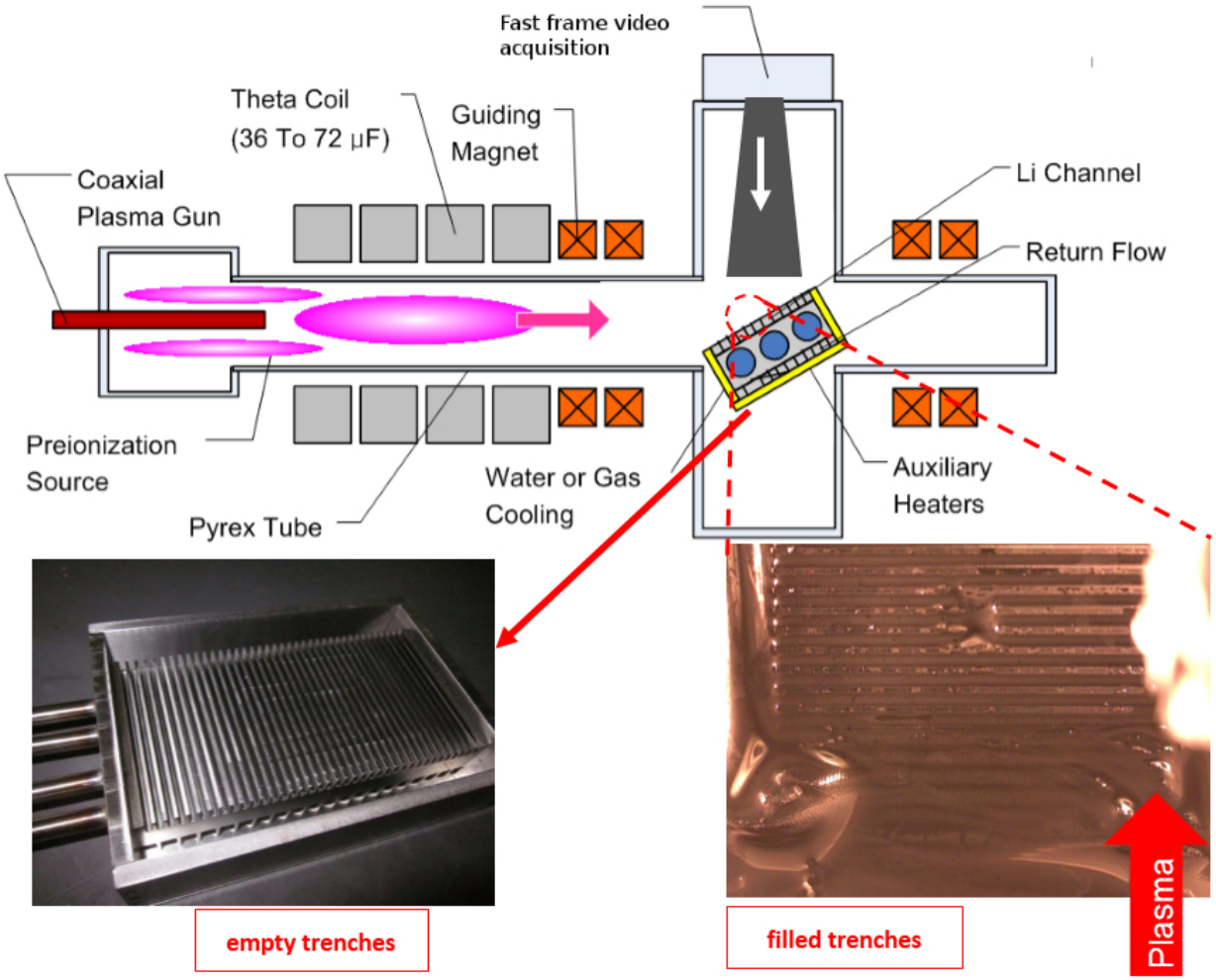

Fig. 3 The schematic of the trench assembly original TELS assembly, which was tested under the plasma flux from DEVEx. The empty trenches and the view of the trenches after being filled with lithium is also shown.

The work with the integrated device – in which an enlarged version of the original LiMIT trench module was combined with the DEVEx linear plasma device, was continued and the flowing lithium surface was exposed to energetic plasma flux of short (few 10 s of µs) durations. The critical dependence on the trench filling on liquid metal ejection during the plasma shots was demonstrated using fast frame camera acquisition.

4. Vertical LiMIT (and beyond).

A smaller set of trenches was used to demonstrate the lithium flow in an arbitrary angle from 0 – 90 deg mounted inside a rotating chamber, and thus proving that the module can be adapted to the real tokamak geometry.

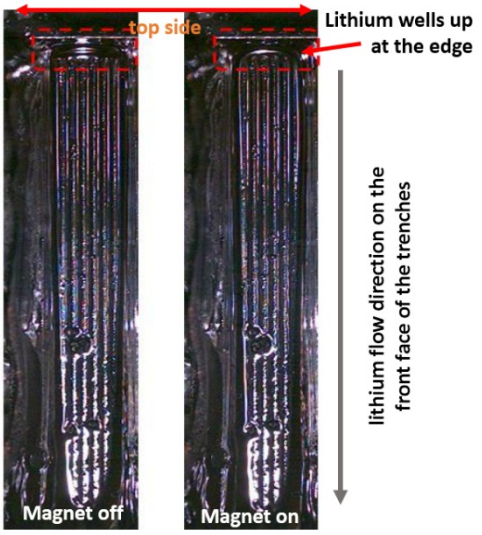

Fig. 4 Evidence of vertical flow attained using the LiMIT module. In the picture, the lithium flows uphill on the underside of the trenches and wells up on the top side, as seen at the edges and then flows downhill on the front face as shown, when the magnetic field is switched on.

Flow could be attained at all orientations between 0 and 90 degrees using the modified experimental setup. The setup has been further modified to orient the module to higher angles (up to 180 degrees). Tests were performed and the operation of trenches by filling up the trenches while the module is kept horizontal and then rotating the setup to orient it in an arbitrary angle all the way up to the inverted state and study the flow characteristics with the external magnetic field turned on were also demonstrated.

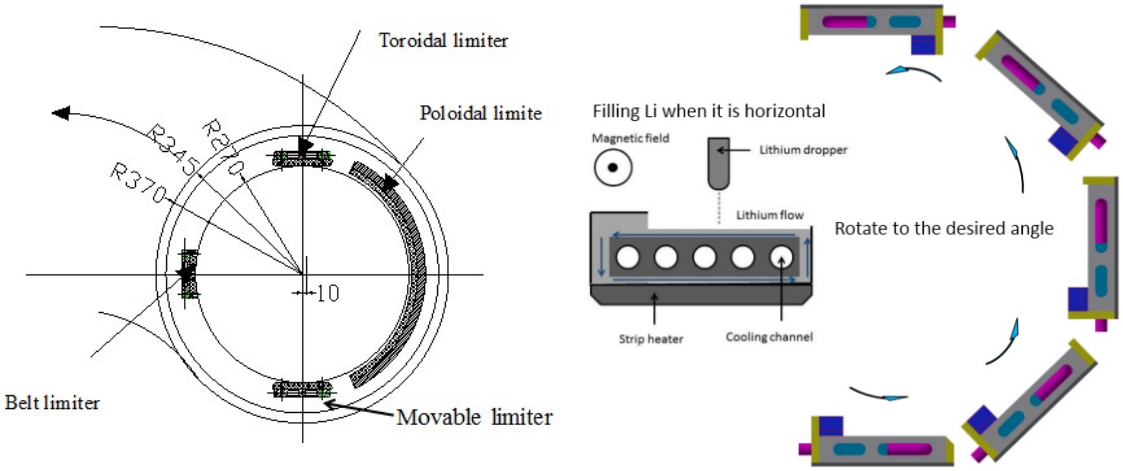

Fig. 5 The limiter configuration in a typical tokamak, and the schematic of the LiMIT module that is currently setup for a full 0 – 180 degree rotation.

2.c Task 1.6

A 3D model on COMSOL was built, as a continuation of the earlier 2D work, and the flow velocity obtained from the model results was compared with the theoretically calculated value. In the model, the infinite long open duct with lithium sheet flowing over the stainless steel trench, driven by the TEMHD driving force was simulated. The x direction represent the trench width (1 mm), the y-direction represent the height of the trench (10 mm) and the z direction is the length. Velocity distribution along x – direction at different positions between the bottom and top surface of the trench (y-direction) and the velocity distribution along the y –direction at the lithium-SS boundary are compared.

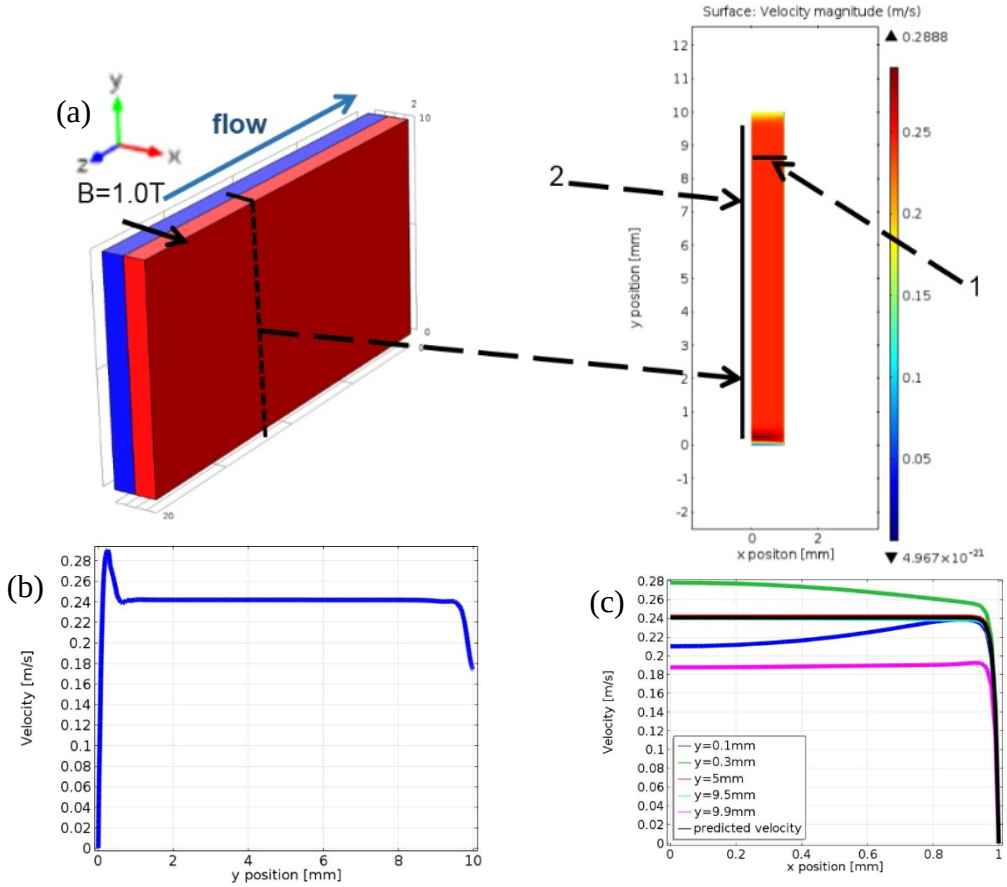

Fig. 6 (a) The COMSOL configuration for the 3D model. Blue region represents the lithium sheet and the red one is the stainless steel trench. Width (x direction) of both parts is 1mm. Height (y direction) is 10mm. Length (z direction) is 20mm. Magnetic field considered B=1.0T along x direction. For the periodic boundary condition, y-z surfaces at x=0 and x=2mm are symmetric surfaces. Also, the top surface is kept at 573K, slip wall, insulated and the bottom surface is at 473K, no slip wall, grounded. (b). The velocity distribution along the y direction at x = 0 and (c) shows the velocity distribution along x direction at different y positions compared with the theoretical value.

From the model, it is inferred that the velocity stays the same for most of the volume inside the trench. A time dependent study of the velocity and temperature profile has also been performed and the results are shown in figure 7.

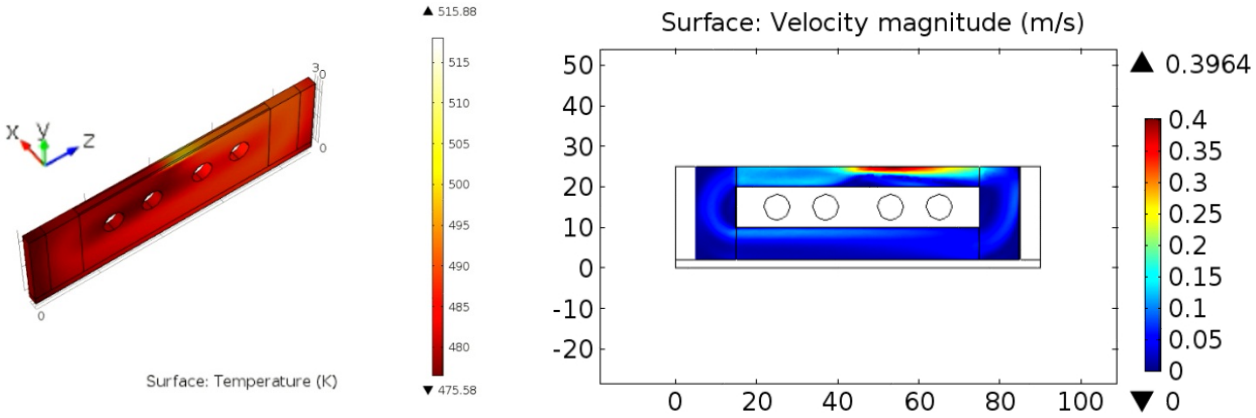

Fig. 7. The temperature and velocity profile after 10 second operation with magnetic field 0.05 T, and an incident heat flux of 500 Wm^{-2} and coolant temperature 293 K.

3. Task 2.4

The effect of pulsed plasma on the flowing metal surfaces was studied using the integrated setup. Data acquisition was made using a fast frame camera. The results indicated that the filling of the trenches was critical to the device performance. The over filled case resulted

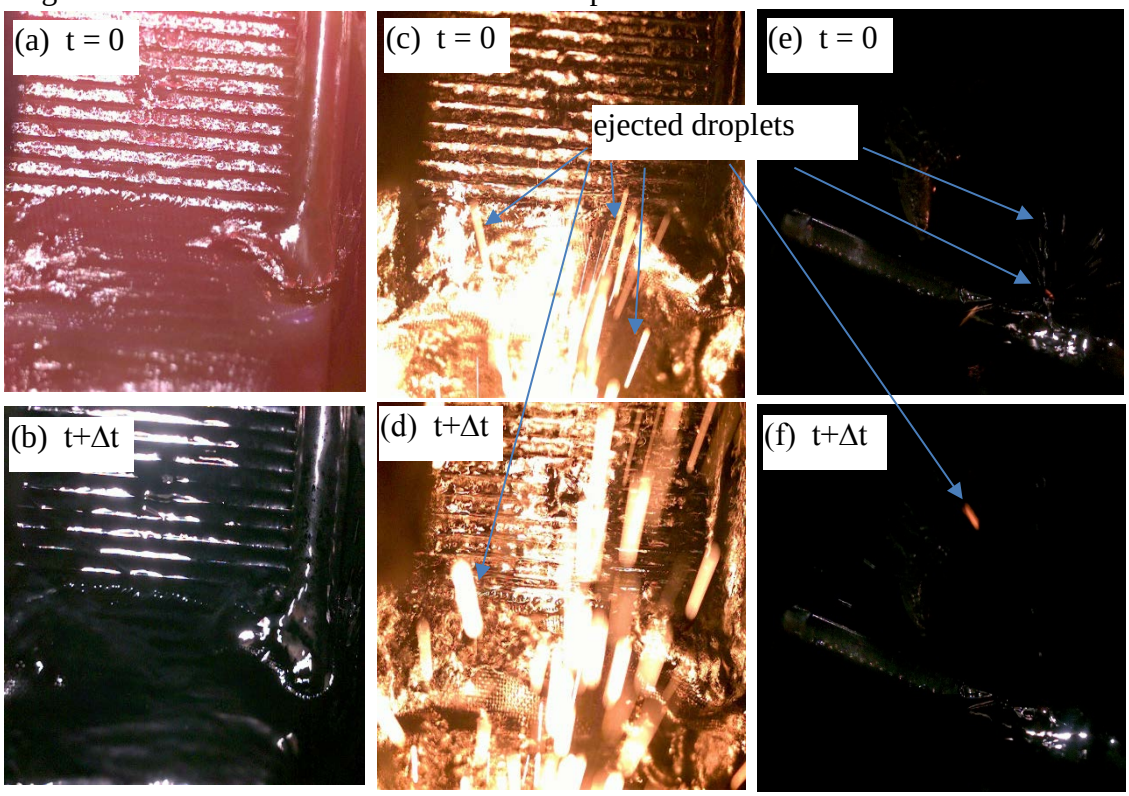

Fig. 8. (a) and (b) The sequential frames from the movie capturing the effect of energetic plasma over the lithium surface when the trenches are filled properly (top view). (c), (d) shows lithum ejection from pools resulting from over filled trenches (top view) and (e) and (f) shows the view from the side.

in pooling of lithium at the bottom region of the tray and significant droplet ejection during

the plasma impact. For the case when the trenches were filled to the correct level, no droplet ejection was observed. The still frames from the acquired movie is shown in figure 7 showing the effect of trench fill on droplet ejection. Hence it was shown that the module with liquid lithium flowing through properly filled trenches can handle transient energetic flux emission from plasma.

4. Task 3.4

The flow velocity was measured as function of the magnetic field (for B = 0.059 T, and B = 0.19 T). The velocity measurement was done by impurity tracking as well as by IR imaging of the top surface of the filled trenches. Figure 9 shows the flowing lithium surface and the measured velocity compared with the theoretically calculated value as a function of the magnetic field.

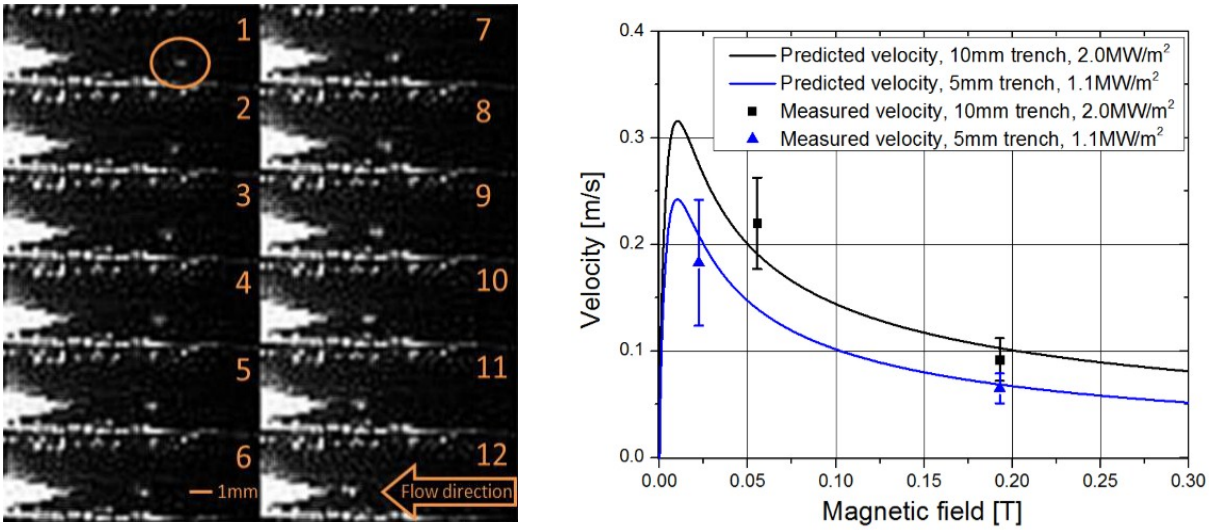

Fig. 9. The velocity measurement done by tracking floating impurities and the measure velocity compared with the theoretically predicted values.

For B = 0.059 T, a value of 0.22 ms^{-1} was obtained and for B = 0.19 T, it was 0.13 ms^{-1}. The measured value matched well with the theoretically predicted ones and hence, by extrapolating, it was expected that the velocity will be 0.053 ms^{-1} for a field of 1 T and 0.035 ms^{-1} for 2 T. Although the results indicated that the flow velocity decreased with increasing magnetic field strength, even for tokamak relevant high magnetic fields, the flow velocity is fast enough to cover the trenches in a matter of seconds.

5. (a,b,c) Task 4 Use of tin and tin-lithium eutectics.

Study was done to obtain a suitable low melting eutectic mixture of tin and lithium, but the alloy obtained had the drawback that the attained melting point was higher (280 °C). Detailed analysis using secondary ion mass spectroscopy (SIMS) of the mixture showed

that lithium was distributed uniformly in the bulk. Due to the high melting point observed, the planned work of using tin and the tin-lithium compound as the working liquid metal for the LiMIT trenches, was not possible. Further investigation is required to determine the best mixture to be used. The SIMS results obtained for the mixture made during one of the trials are shown in figure 10.

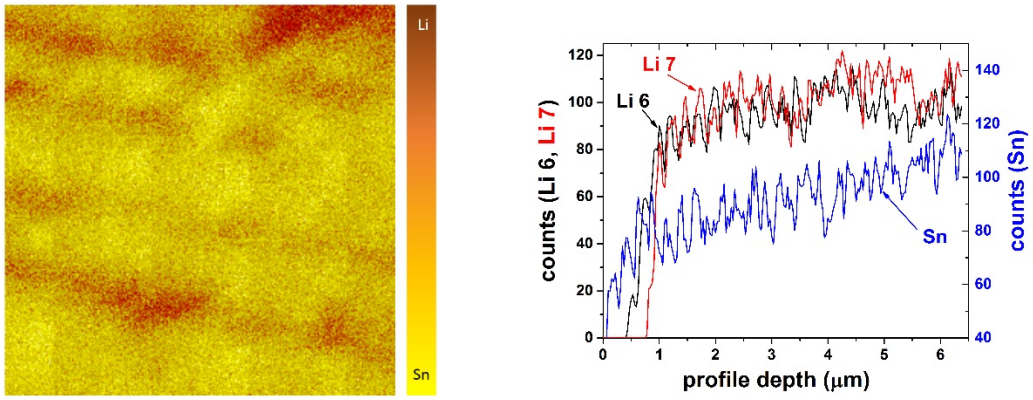

Fig. 10. The surface map of a sample area (1μm x 1μm) showing the concentration of Li and Sn and the ion counts obtained for a depth profile of 6 μm.

The analysis was performed on the samples taken from inside the bulk of the mixture. The initial concentration was 25% Li and 75 % Sn by weight. Further experiments are planned with various other concentrations.

6. No-cost extension period – 2015-2016 (Inputs from additional works)

A still from the fast frame camera (Vision Research Phantom Miro eX4 Color Camera) used to characterize the shots is shown in Figure 11.

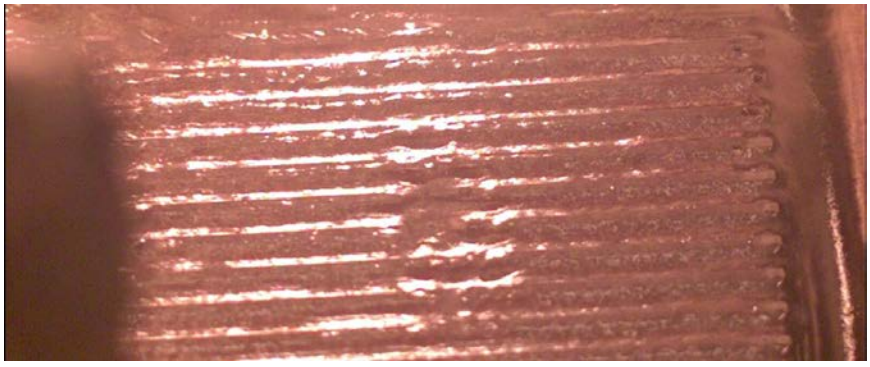

Fig. 11. Lithium in channels in TELS tray immediately after plasma impact, illustrating residual glow from the plasma, as well as waves initiating on the lithium surface. Lithium can be clearly seen to be fully filling the side channels.

In order to gain an understanding of the relative importance of various forces on a free liquid lithium surface, the following Rayleigh-Taylor, Kelvin-Helmholtz analysis was applied to the free surface. This derivation is similar to that put forth by Jaworski [1], but with the addition of Kelvin-Helmholtz instabilities and gravity. A graph illustrating the stability of the lithium surface for different plasma momenta impinging on the target and a current density of 100 kA/m2 in a 0.3T magnetic field (characteristic of NSTX) is shown in fig 12.

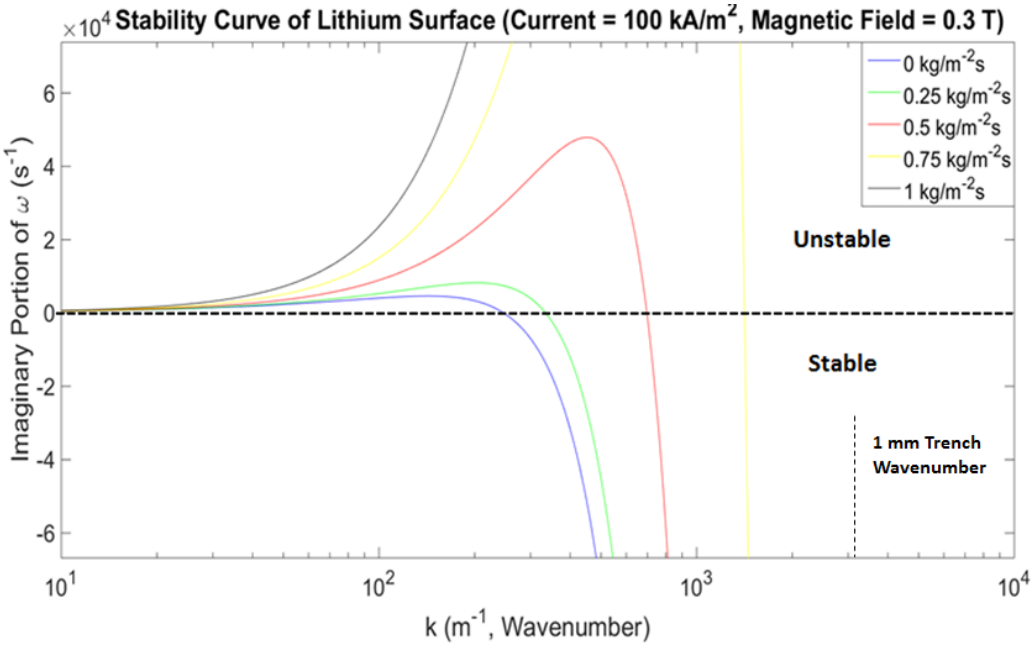

Fig. 12. Stability curve for a liquid lithium free surface exposed to destabilizing JxB forces, stabilizing gravity forces, and flow of plasma across the surface engendering Kelvin-Helmholtz instabilities. It can be seen that for different impinging plasma velocities that the stability for intermediate wavenumbers is dominated by Kelvin-Helmholtz instabilities, however, these are stabilized by restriction to high wavenumber with the use of small lithium channels. Mass flux for several of the theta shots was approximately 0.5 kgm-2s-1.

To properly study the interaction of a free lithium surface with the TELS plasma, it was first required that the TELS plasma be fully characterized. The important drivers in this study will be the JxB forces on the lithium as well as the Kelvin-Helmholtz driven instabilities on the surface. Respectively, the important parameters for each of these are current and magnetic field, and velocity. For the Rayleigh-Taylor like JxB ejection, currents in the lithium need to be well characterized, and the magnetic field must be known. For the Kelvin-Helmholtz driven instabilities, all that need be known is the differential velocity between the plasma and the lithium. In order to measure both of these quantities, a flush probe array was constructed.

Similar to the High-Density Langmuir Probe (HDLP) array installed on NSTX, the probe array constructed here is constructed with a series of probe heads flush with the surface of the PFC that they are embedded in. The probe array discussed herein is referred to as the Circular Flush Probe Array (CFPA). The CFPA consists of 27 active probe heads and one dummy probe head arranged in 3 concentric rings. 8 probes sit in the innermost ring spaced at 45 degree intervals. 12 probes sit in the second ring. 8 are spaced at 45 degree intervals and the remaining 4 are placed evenly between every other of the 8 probes. One of these 4 probes is a dummy probe. The final ring contains the remaining 8 probes at 45 degree intervals. The rings radii are 0.5", 1", and 1.5" respectively. The probes are constructed of ¼" diameter 316 stainless steel rod (McMaster Carr) turned down to 0.1" on one side (front facing) and turned and tapped to 6-32 on the other side (rear facing). The probes are sheathed within ¼" OD ceramic (boron nitride, McMaster Carr) tubes on the turned front side, with the length of the tube cut so that the face of the steel probe is flush with the end of the ceramic tube. The dummy probe is identical to the remainder of the probes, except that the hole in the ceramic standoff is blind rather than through, the steel probe is inserted from the back but is not visible to the plasma. These were in turn mounted on a 4" OD stainless steel disc (316, McMaster Carr) at the intervals prescribed above. Components are locked together with the use of vacuum epoxy (KL-320K, Kurt J. Lesker). The probe array components, before assembly and as seen from the rear can be seen in Figure 13. The assembled probe array as seen from the front can be seen in Figure 14.

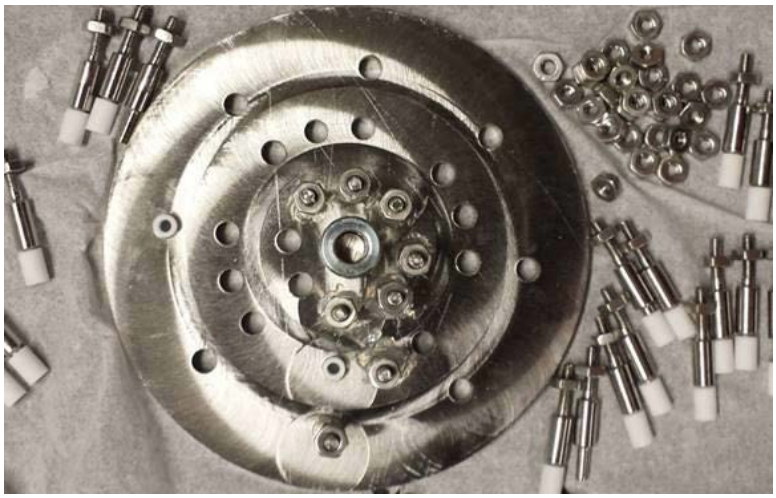

Fig. 13. The flush probe array as seen from the rear. At center is a shaft coupling for mounting to a feedthrough. 8 pins are fully inserted (6 in the inner ring, 1 in the middle ring, 1 in the outer ring). One of the ceramic standoffs is inserted on the left side of the outer ring. The remainder of the probes as well as the nuts used to secure the instrumentation lines are shown scattered around the probe. The diameter of the probe head that is exposed to the plasma is 0.102"

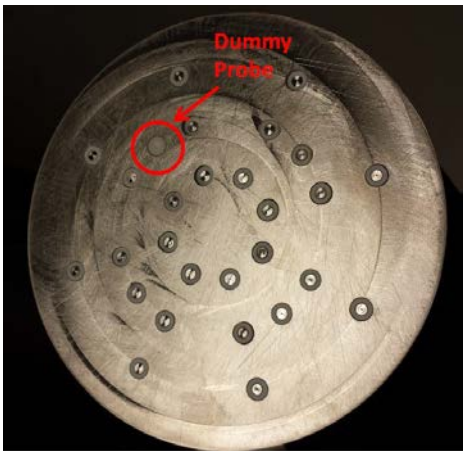

Fig. 14. The CFPA as seen from the front after assembly. The 28 probes are divided into 4 quadrants of 4 probes, with the dummy probe as the middle probe in one of the quadrants. Probes with ceramic sheath can be seen.

Wires attached to the backside of each probe lead from the probe to a vacuum feedthrough and to the analysis circuitry. The entire backside of the probe array including the connecting wires was sheathed in first fiberglass then aluminum tape to shield the signal cables from electromagnetic noise. The aluminum tape continued to the flange, which was ground and therefore the entirety of the aluminum tape sheath was grounded. Currents to each probe head or between probe heads are measured through 2 Ohm, non-inductive resistors (Digikey) with a varistor to prevent damage to the resistor. The voltage across the resistor is measured with a differential amplifier (AD629, Digikey) whose output is read by two oscilloscope (Tektronix TDS2014C and Agilent Infinium 1 GHz). Optionally, an amplifier is used to boost the signal by 5X (OP627). A photograph of the circuit array used to measure 8 simultaneous signals is shown in Figure 15 along with the circuit diagram.

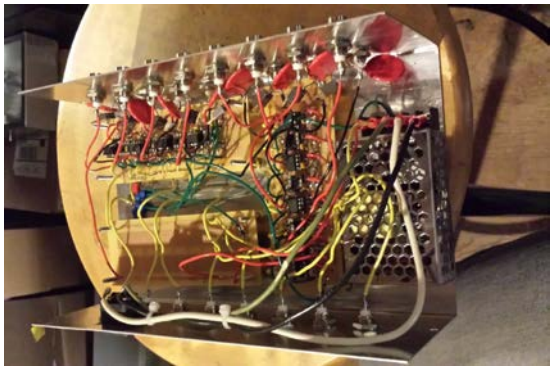

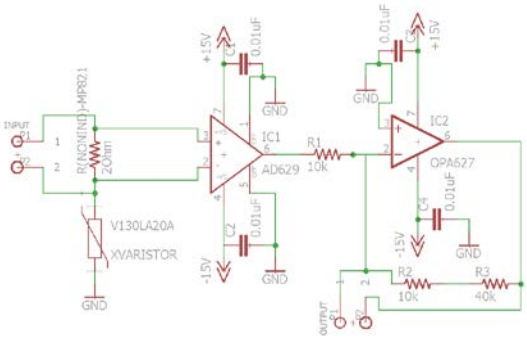

Fig. 15. CFPA analysis circuitry. Perf-board circuits hold the AD629 differential amplifiers, a 12V power supply can be seen on the right side, each non-inductive resistor/varistor combination can be seen across two BNC leads exiting the top of the box. The two inlet BNCs are connected across a non-inductive resistor. Two touch points (OUTPUT P1, OUTPUT P2) are the two outputs, at unity and 5X (inverted) gain.

Axial, radial, and azimuthal currents were measured via connecting the probe heads to each other and to ground in different configurations. By connecting two adjacent probe heads of different radial positions but identical azimuthal positon, a measurement of the radial current was obtained. By connecting two adjacent probe heads of different azimuthal position, but identical radial position, a measurement of the azimuthal current was obtained. Finally, by measuring the current through a resistor between the probe head and ground, a measurement of the axial current was obtained. The dummy probe was used to normalize the axial current signals by subtraction. Since the dummy probe was not exposed to plasma, any current through the dummy probe was attributed to displacement currents. This displacement current was then subtracted from the axial currents measured by the other probes. Since azimuthal and radial currents were measured from probe to probe, it was assumed that the displacement currents would cancel each other out. Typical measured displacement currents were observed to be less than 5% of the total measured current.

Plasma velocity, important for stability to KH instabilities was characterized by analysis of the cross correlation between different current traces, similar to a method used for the characterization of resistive drift waves in the VINETA device at IPP Greifswald [2]. Therefore, the time delay between current signals is also important. Signals offset in time indicate differing arrival times,

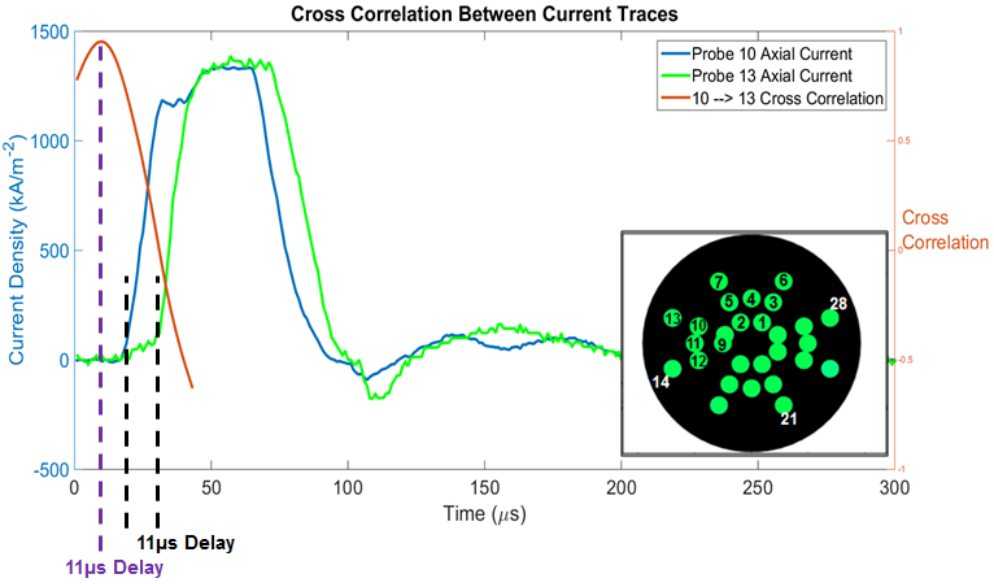

Fig. 16. Sample cross correlation curve between axial current traces, maximum of cross correlation is indicative of time delay between two signals. The distance between two adjacent probes divided by the time delay between the two signals gives the maximum velocity of the plasma across the surface. Double y-axis (left axis is scale for axial current density, blue and green traces; right axis is for cross-correlation, brown trace). Time delay illustrated both between the two axial current traces and for the maximum in the cross correlation curve. Interprobe separation of 12.7 mm divided by 11 µs gives a velocity of 1.15 km/s.

which implies a component of plasma velocity perpendicular to the surface normal e.g. plasma travelling across the surface of the probe array. A maximum on the tangential velocity across the

probe surface between two probe tips is inversely proportional to the time delay between the two signals. As in [105], the time delay between two signals is obtained by way of the cross correlation between the signals. Cross correlation is a measure of how similar two signals are, obtained from a convolution of the two signals divided by a normalizing factor. The cross correlation between two sine waves of the same amplitude, same phase, and same period would be 1. If one of the sine waves were shifted by a phase of pi, the cross correlation would be -1. For the TELS shots performed herein, the cross correlation between different signals was plotted against a time delay applied to one of the signals. The maximum of the cross correlation vs time delay is an indication of the true time delay between two signals. Since the velocity of the plasma has components in the axial, radial, and azimuthal directions, this time delay is a measure of a maximum on the velocity rather than the actual plasma velocity, giving a measure of the maximum KH driving force. A series of typical cross correlation curves for these experiments can be seen in Figure 16. A summary of the cross correlation measurements can be seen in Table 1.

Shot Type	Typical Surface Velocity (km/s) (Calculated)	Maximum Calculated Surface Velocity (km/s)
5.5 kV PiP	4.95±1.18	6
5.5 kV PiP 16 kV Theta	3.6±3	8
6 kV PiP	6±0.75	7
6 kV PiP 16 kV Theta	3.5±3	7.95

Table 1. Calculated surface velocities of the DeVeX plasma on the CFPA from cross-correlation measurements. PiP here is a shortened notation for the coaxial gun. It can be seen that the typical surface velocities decrease with application of the theta pinch, but the maximum velocities increase. The error is taken as the standard deviation of the velocity obtained by cross-correlation measurements.

The velocities measured are primarily radial for the purely coaxial gun shots, and primarily azimuthal for the theta pinch shots. In addition to the cross correlation measurements, the bulk radial and azimuthal velocities could be estimated from the visualizations of the axial currents. The strong increase in current observed at the beginning of the shot was tracked on each channel and by comparing the radial (for the case of the purely coaxial gun shots) and azimuthal (for the case of the theta pinch shots) positions with the time of arrival of current to the probe head, an estimate of the bulk radial and azimuthal speeds could be obtained. The bulk radial speeds for the coaxial gun shots were 4 km/s and 5.6 km/s for the 5.5 kV and 6 kV shots respectively. The bulk

azimuthal speeds for the theta pinch shots were 12.2 km/s and 15.9 km/s for the 5.5 kV coaxial, 16 kV theta and 6 kV coaxial, 16 kV theta shots respectively. The measured speeds from the visualizations for the coaxial gun shots are in good agreement with the speeds as measured by the cross correlation measurements. The results from the current and velocity determinations were used as inputs to the stability determination. The maximum stable dimension is taken as one half of the critical wavelength:

$d_{max}=\pi/k_{crit}$

Two stable dimensions are reported, one using the typical radial and azimuthal currents as measured by the CFPA (reported as Maximum Stable Dimension (mm) Avg.), and the second using the maximum currents as measured by the CFPA (reported as Maximum Stable Dimension (mm) Min.). The results of this analysis are presented in Table 2.

Coax Gun Voltage (kV)	5.5	5.5	6	6
Chamber Static Fill (mTorr)	160	160	160	160
Theta Voltage (kV)	0	16	0	16
Maximum Stable Dimension (mm) Avg.	12	8.3	7.5	5.4
Maximum Stable Dimension (mm) Min.	5.7	6.1	3.7	4.9

Table 2. Maximum stable dimension of a lithium free surface under exposure to the DeVeX plasma under various shot conditions. Presented are the results of the stability analysis for both the typical values of the currents and velocities (tagged as average) as well as the maximum values of the currents and velocities (tagged as minimum in reference to the absolute minimum expected dimension over which there may be ejection of lithium).

This table shows the maximum stable dimension of a lithium free surface when exposed to the TELS plasma for 5.5 kV and 6 kV coaxial gun shots with and without use of the theta pinch. It can be seen that the expected threshold stable dimension is smaller for the theta pinch shots if the typical values are determinant of the maximum stable dimension, and larger for the theta pinch shots in the case that the maximum values are the determinant of the maximum stable dimension. The stable dimension, however, for all of the conditions detailed above is in the range of 3.5 to 12 mm. Experimental determination of the correct parameters is undertaken to verify the analysis.

Figure 17 TELS tray during plasma impact from the DeVeX plasma. (Side view of channels).

A series of LiMIT trenches were machined with different trench widths ranging from 1 to 14 mm in width. A picture and side-view schematic of these trenches can be seen in Figure 18. Trenches were milled from a block of 316 stainless steel. Side and bottom panels were also milled from 316 stainless steel bar. Cartridge heaters installed in a 316 stainless steel block below the bottom panel serve to heat the LiMIT device. Two thermocouples one inserted into the trenches and one on the back face of the heating block monitor the temperature of the system.

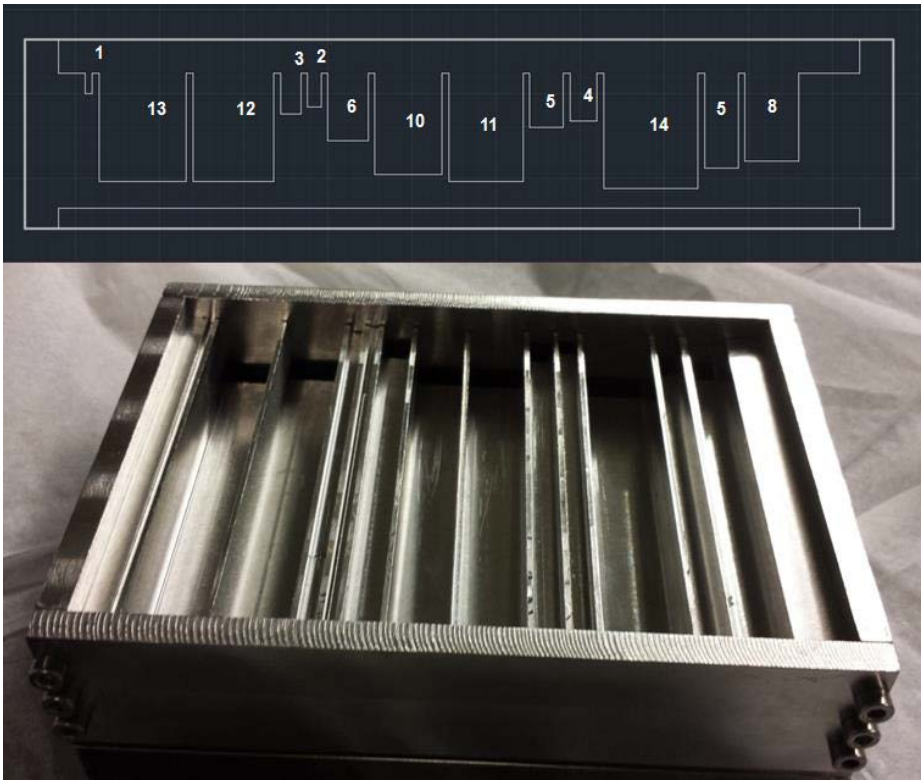

Figure 18. (Top) Schematic of the side view of the special LiMIT channels. Trench width is displayed in millimeters. (Bottom) Photograph of the LiMIT trenches as assembled. Trenches were subsequently installed into the TELS chamber and filled.

This LiMIT structure was then installed into TELS, filled with lithium and a series of plasma shots (identical to the current characterization ones) were fired upon the trenches. To increase visibility during these shots, a bake lamp was employed to illuminate the chamber and the fast frame camera was run in a “Low Light” mode which enabled longer exposure times. Series of still frames were captured from the campaign and lithium ejection was monitored. During these shots, when the trenches were completely wetted by lithium, however, none of the trenches showed ejection under any of the shot conditions. A fast frame still can be seen in figure 19, showing no ejection from

the 1-14 mm trenches. For the repeated tests with under-filled and improperly wetted trenches, droplet ejection was observed from lithium pools outside the trenches. Still frames of the fast frame videos from the series of shots of the unwetted trenches were analyzed and the ejected lithium particles are ray-traced back to their source. Ejected particles from each of the unwetted shots were ray-traced back to only the 10 and 11 mm trenches as well as the lithium pool in the front of the trenches. These ejected particles are assumed to be from the unwetted droplets in each of the 10

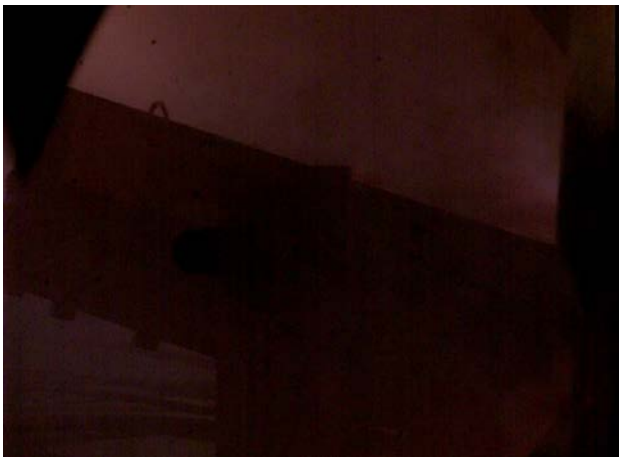

Figure 18. Still frame from the shots fired upon the 1-14 mm trenches showing no ejection from the lithium channels (6 kV coaxial gun, 0 kV theta pinch). Trenches viewed from the side as in 6.5, holding frame was adjusted between 6.5 and 6.6 to better support the trenches within the TELS device and to allow arbitrary rotation. Filling occurred while channels were at 00. Trenches were then rotated for plasma exposure. Frame illuminated by afterglow of plasma.

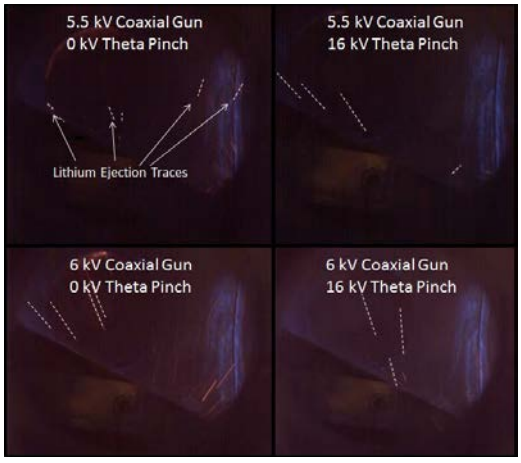

Figure 19. Ejection observed from the 10 and 11 mm trenches as well as the lithium pool in the bottom of the trenches. Increased ejection is observed in the case of the 6 kV coaxial gun shots, however, it is still only observed to be coming from the 10 and 11 mm trenches and the lithium pool.

and 11 mm trenches (as well as the unwetted pool of lithium). Ejection was seen in the cases of

the 5.5 and 6 kV coaxial gun shots with and without the theta pinch. Stills of the ejection from these shots are shown in Figure 19.

The lack of ejection from the 1-14 mm trenches demonstrates that the initial RT-KH stability boundary underestimates the maximum stable trench dimension. Consequently, a series of larger trench dimensions were sought to properly capture the location of the experimental stability boundary. A diagram of the modified cross section is shown in Figure 20.

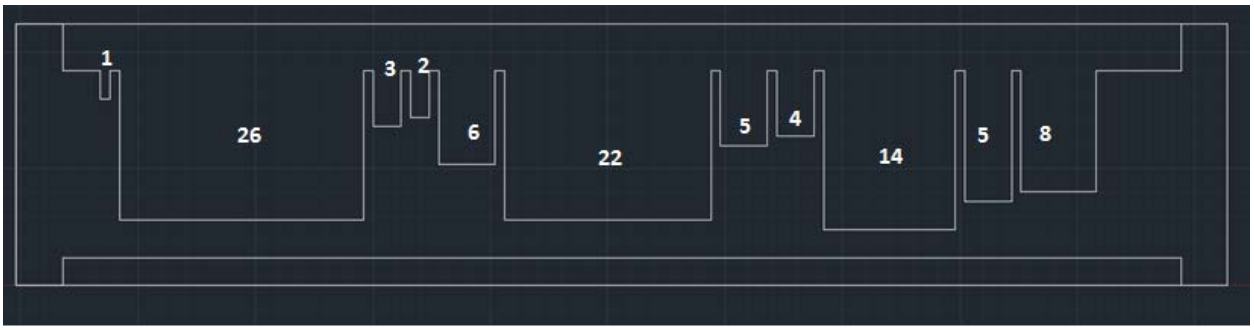

Figure 20. Modified TELS trenches with wider trenches in place of the 10, 11, 12, and 13 mm trenches. Wall between 12 and 13 mm trenches milled out to form the 26 mm trench. Wall between the 10 and 11 mm trenches milled out to form the 22 mm trench.

This modified LiMIT structure was then installed into DeVeX and the same series of plasma shots were fired upon the trenches. Significant ejection from the lithium pool, which included the 26 mm trench, at the base of the TELS trenches was observed during exposure to the DeVeX plasma shots. Figure 21 shows the still frame from one of the plasma shots showing lithium ejection.

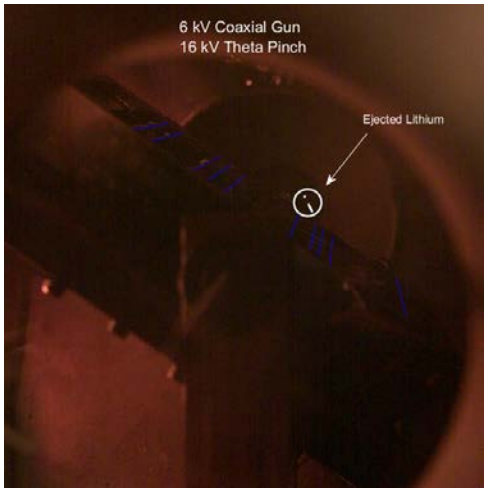

Figure 21. Ejection of lithium from the TELS trenches after exposure to the 6 kV coaxial, 16 kV theta pinch shot. Ejection observed from edge of lithium pool, but above the boundary of the 26 mm trench.

However, no ejection was observed from the 22mm trench, indicating that the stability boundary is greater than 22 mm, and lies in the neighborhood of 26 mm for each of the shot conditions investigated. Ejection of lithium was strongest from the 6 kV coaxial gun shots. Ejection was also observed to be greatest from the edges and corners of the trenches. Only under the 6 kV coaxial gun shots was lithium observed to eject from the trench center. It is clear from these tests however, that the experimental stability boundary of lithium deviates significantly from the derived analytic stability boundary.

7. Conclusion from the extended study: A variety of trench structures were exposed within the TELS chamber to the DeVeX plasma gun. It was found that ejection depended on a multiple of variables, some not immediately obvious. The first of these influences to be observed was wetting of the lithium trenches. Under unwet conditions, the lithium ejected droplets readily under plasma exposure. Variable width trenches inserted into the chamber to investigate the dependence of the stability boundary on trench dimension during wetted conditions showed results that were considered anomalous at first. However, after repeated exposures to similar conditions, it was seen that the linear stability theory was incorrect in its description of the physics undergone by lithium under transient plasma exposure. Trenches between 1 and 14 mm in width did not eject under multiple tests, even when the trenches were reversed to investigate if the effect was purely due to spatial variation of the plasma on target. Subsequent exposure of much larger trenches showed strong evidence of lithium ejection under all tested plasma exposure conditions. Strongest ejection was observed during the 6 kV coaxial gun 0 kV theta shots, which is commensurate with the shot conditions under which the largest radial/azimuthal currents were delivered to the CFPA, suggesting that the current driven instabilities dominate over the plasma velocity driven instabilities for the trench dimensions investigated in this work.

8. Further work

Two of the initial tasks could be further investigated thoroughly during future works planned. They are,

1. designing porous capillary structures which will be utilized for containing the liquid metal and also will allow TEMHD driven flow
2. use of tin as an alternative for lithium as the flowing liquid metal, and synthesizing a suitable low melting eutectic mixture of tin and lithium, and evaluating its performance in the LiMIT trenches.

The former task will establish an alternative design for the proposed open trench LiMIT design. Based on the excellent results obtained from the tests using the open trench design, all the work done can be focused on that design, aimed at evaluating its performance in tokamak relevant plasma conditions. For the latter task, suitable number of trials need to be performed to identify a

low melting tin-lithium eutectic mixture that can be used in the trenches. Both these tasks will be quite relevant for advancing the liquid PFC concept.

References

[1] M.A. Jaworski et.al. Liquid lithium divertor characteristics and plasma-material interactions in NSTX high-performance plasmas. *Nucl. Fus.* **53** 083032 (2013).
[2] C. Schroder. Experimental investigations on drift waves in linear magnetized plasmas. Doctoral thesis, Ernst-Moritz-Arndt-Universitat Greifswald, (2003).